AIP Applied Physics Letters

Correlation between the microstructure and electroluminescence properties of Er-doped metal-oxide semiconductor structures

A. Kanjilal, L. Rebohle, W. Skorupa, and M. Helm

Citation: Applied Physics Letters **94**, 101916 (2009); doi: 10.1063/1.3098474
View online: http://dx.doi.org/10.1063/1.3098474
View Table of Contents: http://scitation.aip.org/content/aip/journal/apl/94/10?ver=pdfcov
Published by the AIP Publishing

Articles you may be interested in

Blue and red electroluminescence of Europium-implanted metal-oxide-semiconductor structures as a probe for the dynamics of microstructure
Appl. Phys. Lett. **93**, 071908 (2008); 10.1063/1.2964176

Switchable two-color electroluminescence based on a Si metal-oxide-semiconductor structure doped with Eu
Appl. Phys. Lett. **90**, 181121 (2007); 10.1063/1.2735285

Improved blue-green electroluminescence of metal-oxide-semiconductor diode fabricated on multirecipe Si-implanted and annealed SiO 2 / Si substrate
J. Appl. Phys. **95**, 8484 (2004); 10.1063/1.1739283

Hot electron impact excitation cross-section of Er 3+ and electroluminescence from erbium-implanted silicon metal-oxide-semiconductor tunnel diodes
Appl. Phys. Lett. **71**, 2824 (1997); 10.1063/1.120147

Room-temperature photoluminescence and electroluminescence from Er-doped silicon-rich silicon oxide
Appl. Phys. Lett. **70**, 1790 (1997); 10.1063/1.118693

This article is copyrighted as indicated in the article. Reuse of AIP content is subject to the terms at: http://scitation.aip.org/termsconditions. Downloaded to IP: 136.160.185.105 On: Mon, 15 Dec 2014 03:55:57

Correlation between the microstructure and electroluminescence properties of Er-doped metal-oxide semiconductor structures

A. Kanjilal,[a] L. Rebohle, W. Skorupa, and M. Helm
Institute of Ion Beam Physics and Materials Research, Forschungszentrum Rossendorf, P.O. Box 51 01 19, 01314 Dresden, Germany

(Received 16 December 2008; accepted 22 February 2009; published online 13 March 2009)

Optical response of a rare earth (RE)-doped SiO_2 layer is known to deteriorate markedly at room temperature due to RE clustering. The key challenge is therefore to probe the ongoing processes at the microscopic level and the subsequent impact on the luminescence properties with increasing RE concentration. Here, we report how the Er electroluminescence in a metal-oxide-semiconductor structure has been affected by increasing Er content. Our results indicate that the Er oxide clustering is anticipated by the formation of Si-based oxygen-deficiency centers during postimplantation annealing and leads to a strong quenching of the short-wavelength (350–500 nm) Er electroluminescence. © *2009 American Institute of Physics*. [DOI: 10.1063/1.3098474]

Although silicon based light emitters have been realized by utilizing nanoscale structures,[1,2] the efficiency of such devices is far from the practical application. In fact, electrically pumped light-emitting devices (LEDs) are highly desirable from the optoelectronic standpoint. In spite of considerable progress in nanotechnology the introduction of the rare earth (RE) doped metal-oxide-semiconductor LEDs (MOSLEDs) (Ref. 2) gives an auxiliary platform, where the RE-based electroluminescence (EL) is controlled by the intrashell transitions in partially filled shells.[3] For instance, the intra-4f shell transition ($^4I_{13/2} \rightarrow {}^4I_{15/2}$) of Er^{3+} can emit an infrared (IR) light at $\sim$1.53 μm.[4] We must note here that while most of the intraband transitions are optically forbidden for RE ions, no such constraint exists during electrical pumping; hence, several EL signals can be expected during electron injection. The temperature and concentration quenching of RE luminescence remain the major limiting factors to achieve maximum efficiency at room temperature (RT).[2] Owing to low solubility of the RE elements in SiO_2,[5] a significant fraction of RE ions generally prefer to form clusters during postimplantation annealing.[4] In this letter we demonstrate the evolution of microstructure in Er-doped MOSLEDs as a function of Er concentration, [Er], and underscore its influence on Er electroluminescence.

Among various approaches, ion implantation is recognized as a powerful method owing to its excellent control over distribution of dopants and residual defect.[4] Here, the Er-implanted MOS structures were fabricated by standard local oxidation of silicon (LOCOS) technology with a 200 nm thick thermally grown SiO_2 layer on n-type Si(100) wafers, where the 250 keV Er ions with fluences in the range of $(1-5)\times 10^{15}$ ions/cm^2 were implanted using a typical target current density of $\sim$200 nA/cm^2. Initially, the Er concentration was determined to be in between 0.3% and 1.4% at R_p ($\sim$115 nm) by the SRIM-2006 calculations,[6] which was later confirmed by Rutherford backscattering spectroscopy measurements. The samples were subjected to furnace annealing for 30 min at 900 °C in nitrogen ambience. $\sim$100 nm thick silicon-oxynitride (SiON) layer was deposited on top of the LOCOS structure. In addition, a semitransparent indium-tin oxide and aluminum contacts were sputter deposited in the front and rear surfaces, respectively. Arrays of circular electrodes (diameter of $\sim$300 μm) were developed on the front surface by optical lithography. All the RT EL spectra, recorded in constant current mode and under forward bias condition, were detected by a monochromator in combination with a photomultiplier or a liquid nitrogen cooled InGaAs detector. The photomultiplier in combination with a photon counting system were employed to study the time-resolved EL dynamics. Cross-sectional transmission-electron-microscopy (TEM) images were taken by a FEI Titan S/TEM, operating at 300 keV.

Figure 1(a) shows the EL spectra, recorded with a constant current density (J) of $\sim$7.1 mA/cm^2 for the MOSLEDs containing 0.3%, 0.8%, and 1.4% Er. The inset projects another visible range spectrum from a *different* set of MOSLEDs containing 0.5% Er for J=70.7 mA/cm^2. Although the implantations have been carried out at RT, the difference in EL spectra implies that the signal is very sensitive to the sample preparation conditions (such as SiO_2 and SiON layer thicknesses, implantation energy, target current density, Er concentration, etc.). The EL bands peaking at $\sim$387, 412, 437, 478, 527, 551, and 660 nm (marked by vertical lines) can be assigned as the radiative transitions from the $^2G_{11/2}$, $^2H_{9/2}$, ($^4F_{3/2}$+$^4F_{5/2}$), $^4F_{7/2}$, $^2H_{11/2}$, $^4S_{9/2}$ and $^4F_{9/2}$ states to the ground $^4I_{15/2}$ state of Er^{3+}, respectively.[3] Note that the cut-off wavelength of the photomultiplier is $\sim$370 nm, which may affect the 387 nm Er peak. The IR peak at $\sim$1535 nm is the characteristic feature of the $^4I_{13/2} \rightarrow {}^4I_{15/2}$ transition in Er^{3+}.[7] Nevertheless, the 437 and 478 nm EL signals are indistinguishable in the present set [main part of Fig. 1(a)] up to 0.8% Er. Apparently, a broad EL band at $\sim$460 nm (indicated by *downward arrow*) that evolves by suppressing the Er EL signals in the range of 350–500 nm for 1.4% Er can be attributed to the Si-based oxygen-deficiency centers (SiODCs).[1] Since the 1535 nm Er EL intensity is almost saturated at $\sim$0.8% Er, MOSLEDs made of 0.8% Er are considered to be the best-emitting electrical structures.

The visible range EL spectrum has been monitored as a function of J for the 0.8% Er-doped MOSLEDs [Fig. 1(b)]. As evident, the intensity of the short wavelength Er peaks, especially the 412 nm EL becomes more prominent with increasing J, signifying efficient excitation of the $^2H_{9/2}$ or the

[a]Electronic mail: a.kanjilal@fzd.de.

This article is copyrighted as indicated in the article. Reuse of AIP content is subject to the terms at: http://scitation.aip.org/termsconditions. Downloaded to IP: 136.160.185.105 On: Mon, 15 Dec 2014 03:55:57

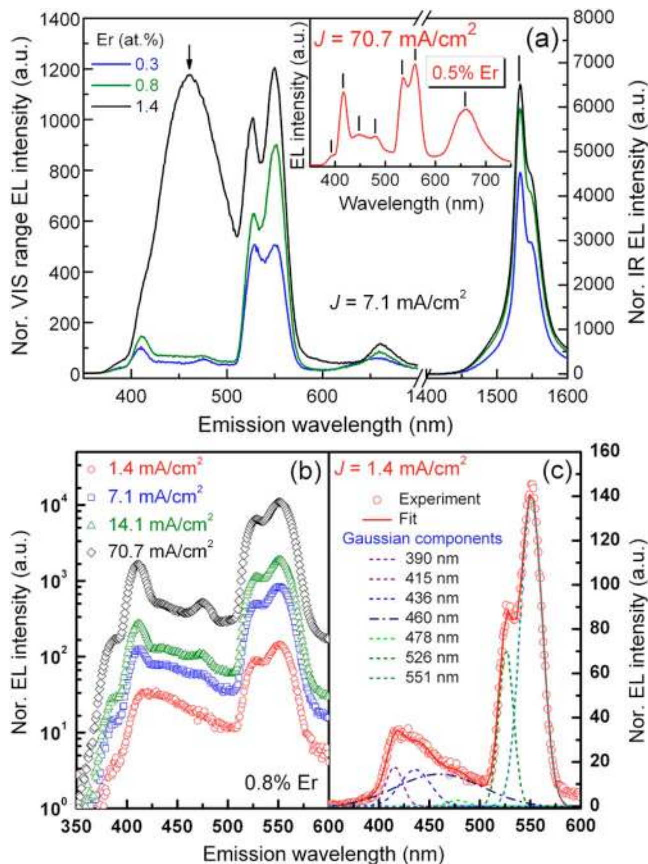

FIG. 1. (Color online) The visible and IR EL spectra recorded from MOSLEDs with 0.3%, 0.8%, and 1.4% Er (a). Another spectrum for 0.5% Er is shown in inset (a) Visible EL spectra for 0.8% Er with increasing J are displayed by open symbols (b). Deconvoluted Er peaks (dashed curves) and the 460 nm band (dash-dot curve) together with fit (solid curve) are superimposed on the experimental data for $J=1.4\ \mathrm{mA/cm^2}$ (c).

states above Er^{3+} by hot electrons and subsequent relaxation back to the ground $^4I_{15/2}$ state.[3] The experimental data for $J=1.4\ \mathrm{mA/cm^2}$ is well reproduced using seven Gaussian bands with peak maxima at 390, 415, 436, 460, 478, 526, and 551 nm, respectively [see Fig. 1(c)]. Clearly, except the 460 nm Gaussian band, other components are near to the expected peak positions of Er^{3+} ions, as stated above.[3] The fitting procedure, therefore, confirms the coexistence of both Er-related emissions and the SiODC-induced EL at ~460 nm,[1] where the peak intensity for the latter one dominates further by introducing additional Er [see Fig. 1(a)]. Based on the EL results, we believe that the ion beam induced defects in SiO_2, especially those based on a local deficiency of oxygen, cannot be removed completely during postimplantation annealing.

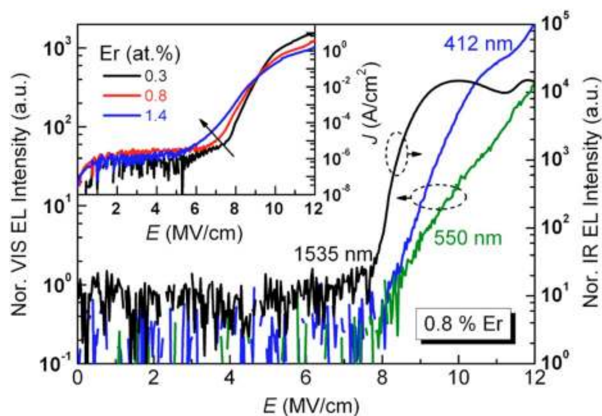

FIG. 2. (Color online) The EL intensity of the 412, 550, and 1535 nm Er peaks with increasing electric field for 0.8% Er. The inset exhibits Er concentration dependent J-E characteristics.

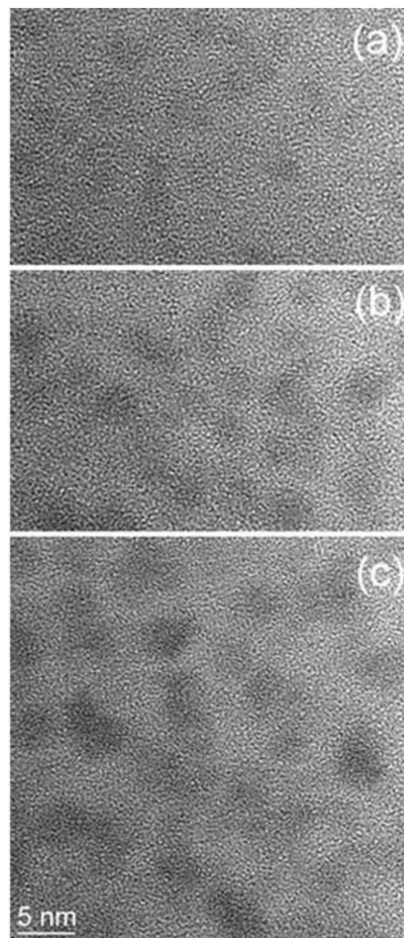

FIG. 3. High-resolution TEM images for 0.3% (a), 0.8%, (b) and 1.4% (c) Er. The dark contrast in gray background represents Er oxide clusters. The average cluster size is estimated to be ~2.1 nm (a), 3.8 (b), and 5.3 nm (c) near R_p. All TEM images are in the same scale.

In order to follow the electric field (E) dependent excitation mechanism of Er^{3+}, the 412, 550, and 1535 nm EL bands have been chosen due to their prominent feature. The respective EL intensity dependence is monitored for the MOSLEDs containing 0.3% and 0.8% Er, where the profiles for the latter case are exhibited in Fig. 2. Apparently, the Er^{3+} ions do not emit light below 7.5 MV/cm, while the trends of the $^2H_{9/2}\rightarrow{}^4I_{15/2}$ (blue), $^4S_{9/2}\rightarrow{}^4I_{15/2}$ (green), and $^4I_{13/2}\rightarrow{}^4I_{15/2}$ (black) EL intensity curves are almost independent to each other. From the energy level standpoint in Er^{3+},[3] it is expected that the first excited state ($^4I_{13/2}$) can be excited efficiently by relatively lower E value than the other high energy states. In fact, the 1535 nm EL intensity starts increasing much earlier than the 412 and 550 nm bands and saturates faster. The inset of Fig. 2 summarizes the J-E characteristics of the working devices, confirming the device integrity even after device processing. A small displacement current is measured in lower electric fields, where the experimental data can be fitted by a power law $J=A_1E^m$ for $0.5<m<0.7$. This observation is analogous to the Si-rich nitride/Si superstructures,[8] and hence the electron injection can be explained in the light of space charge limited conduc-

This article is copyrighted as indicated in the article. Reuse of AIP content is subject to the terms at: http://scitation.aip.org/termsconditions. Downloaded to IP: 136.160.185.105 On: Mon, 15 Dec 2014 03:55:57

TABLE I. Results of the decay time (τ_d), dispersion factor (β), and the $\sigma\tau$ analysis for different Er EL bands with increasing [Er].

Emission wavelengths (nm)	$\tau_d(\mu s) \pm 5\%$ Er conc. (at. %)			$\beta \pm 5\%$ Er conc. (at. %)			$\sigma\tau(cm^2\ s) \pm 5\%$ Er conc. (at. %)		
	0.3	0.8	1.4	0.3	0.8	1.4	0.3	0.8	1.4
412	207	267	⋯	0.56	0.41	⋯	1.0×10^{-20}	8.2×10^{-21}	⋯
460	⋯	⋯	4867	⋯	⋯	0.81	⋯	⋯	3.3×10^{-18}
550	232	239	274	0.47	0.44	0.50	2.1×10^{-20}	3.2×10^{-22}	8.8×10^{-21}

tion to the SiON layer in the low electric field region. Here, m depends on the energy width of the trap distribution in SiON, while A_1 is a constant. Above this electric field region, the J-E characteristic shows an almost exponential behavior. As evident, the threshold E moves toward the lower value with increasing [Er], suggesting a decrease in barrier height at the Si/SiO_2 interface.[9] While the charge transport from the conduction band (CB) of Si to the CB of SiO_2 layer is found to be mainly governed by the Fowler–Nordheim tunneling in higher E values, the contribution from other mechanisms such as Poole–Frenkel emission, hopping, charging, etc., has also been noticed.[10]

It is known that the SiO_2 network is destroyed during ion implantation and displaces Si and oxygen (O) atoms. The displaced Si and O atoms may either be absorbed into the local SiO_2 network or diffused to the impurity (Er) sites for achieving a stable composition. According to the formation enthalpies of SiO_2 (−856.3 kJ/mol) and Er_2O_3 (−1808.7 kJ/mol),[11] a close competition in reconstructing SiO_2 and Er_2O_3 configurations is expected. Indeed, a considerable fraction of Er atoms are involved in developing amorphous Er oxide clusters[4,5] (Fig. 3) during annealing and eventually trigger the formation of SiODCs. However, due to the presence of the surrounding SiO_2 networks, it is impossible to draw a conclusion over the exact composition of the Er oxide clusters. Discernibly, the average size of such Er oxide clusters gradually increases from ~2.1 to 5.3 nm at R_p with increasing [Er]. Note that the Er oxide clusters are more or less distributed over a region of ~80 nm in the central part of the SiO_2 layer. The decay time (τ_d) of the prominent EL peaks (Table I) has also been estimated using a *stretched* exponential[12] $I(t) \propto \exp[-(t/\tau)^{\beta}]$, where β is a dispersion factor indicating a spread of Er lifetime (τ) due to the presence of different Er sites.[13] The product of the excitation cross-section (σ) and τ has been calculated according to Ref. 14, evidencing overall quenching of σ with increasing cluster size. Interestingly, the decay times for the blue and green EL bands are found to increase with increasing [Er], which is just opposite to the known phenomenon of concentration quenching.[15] Since the contribution of the SiODCs dominates over Er emission [see Fig. 1(a)] and the average size of Er oxide clusters is found enhancing simultaneously with increasing [Er] (Fig. 3), it seems that a delicate balance between the SiODCs near the cluster surface and the cluster size itself plays the pivotal role in controlling EL. Indeed, the electric field would be lower within an Er oxide cluster than in SiO_2 as the dielectric constant of the Er_2O_3 (~13) (Ref. 16) is higher than that of SiO_2 (3.9).[10] The relatively weak field in an Er oxide cluster cannot accelerate electrons efficiently in order to excite the Er^{3+} ions. Hence, the Er^{3+} ions residing near to the core region of a cluster are assumed to be inactive, whereas the ions situated at the surface can predominantly take part in EL. Although the increase in cluster size reduces the number of surface Er^{3+}, the subsequent increase in cluster density by enhancing [Er] (Fig. 3) is expected to compensate the lack of excitable Er^{3+} ions. Moreover, Er^{3+} ions in the core region of a cluster might be excited electrically if relatively high electric field, like above 11 MV/cm, is applied for the blue and IR EL profiles (Fig. 2).

In conclusion, we have demonstrated the EL properties of the Er-doped MOSLEDs with increasing [Er] up to 1.4% by lowering the barrier height at the Si/SiO_2 interface. The variation in EL output has been illustrated on the ground of increasing average sizes of the Er oxide clusters as a function of [Er], leading to the formation of the SiODCs in SiO_2. In fact, the SiODC induced 460 nm EL dominates over the short wavelength (350–500 nm) Er signals with increasing [Er].

We thank the Rossendorf Implantation Group for ion implantation and H. Felsmann, C. Neisser, and G. Schnabel for their careful semiconductor preparation work. The support of the Alexander von Humboldt Foundation is gratefully acknowledged.

[1] L. Rebohle, J. von Borany, R. A. Yankov, W. Skorupa, I. E. Tyschenko, H. Fröb, and K. Leo, Appl. Phys. Lett. **71**, 2809 (1997).
[2] L. Rebohle, J. Lehmann, S. Prucnal, A. Kanjilal, A. Nazarov, I. Tyagulskii, W. Skorupa, and M. Helm, Appl. Phys. Lett. **93**, 071908 (2008).
[3] G. H. Dieke, *Spectra and Energy Levels of Rare Earth Ions in Crystals* (Interscience, New York, 1968), Chap. 13.
[4] A. Kanjilal, L. Rebohle, M. Voelskow, W. Skorupa, and M. Helm, J. Appl. Phys. **104**, 103522 (2008).
[5] J. Lægsgaard, Phys. Rev. B **65**, 174114 (2002).
[6] J. F. Zeigler, SRIM-2006.02 (http://www.srim.org).
[7] B. Garrido, C. García, S.-Y. Seo, P. Pellegrino, D. Navarro-Urrios, N. Daldosso, L. Pavesi, F. Gourbilleau, and R. Rizk, Phys. Rev. B **76**, 245308 (2007).
[8] J. Warga, R. Li, S. N. Basu, and L. Dal Negro, Appl. Phys. Lett. **93**, 151116 (2008).
[9] L. Rebohle, J. von Borany, H. Fröb, and W. Skorupa, Appl. Phys. B **70**, 131 (2000).
[10] T. Hori, *Gate Dielectrics and MOS ULSIs: Principle, Technologies, and Applications* (Springer, Berlin, 1997).
[11] *CRC Handbook of Chemistry and Physics*, 87th ed., edited by D. R. Lide (CRC, Boca Raton, 2006).
[12] L. Pavesi and M. Ceschini, Phys. Rev. B **48**, 17625 (1993).
[13] G. Franzò, E. Pecora, F. Priolo, and F. Iacona, Appl. Phys. Lett. **90**, 183102 (2007).
[14] A. Nazarov, J. M. Sun, W. Skorupa, R. A. Yankov, I. N. Osiyuk, I. P. Tjagulskii, V. S. Lysenko, and T. Gebel, Appl. Phys. Lett. **86**, 151914 (2005).
[15] G. Franzò, D. Pacifici, V. Vinciguerra, F. Priolo, and F. Iacona, Appl. Phys. Lett. **76**, 2167 (2000).
[16] Y. Y. Zhu, R. Xu, S. Chen, Z. B. Fang, F. Xue, Y. L. Fan, X. J. Yang, and Z. M. Jiang, Thin Solid Films **508**, 86 (2006).

This article is copyrighted as indicated in the article. Reuse of AIP content is subject to the terms at: http://scitation.aip.org/termsconditions. Downloaded to IP: 136.160.185.105 On: Mon, 15 Dec 2014 03:55:57